communications earth & environment

ARTICLE

https://doi.org/10.1038/s43247-023-01197-3 OPEN

Light oxygen isotopic composition in deep mantle reveals oceanic crust subduction before 3.3 billion years ago

Dongjian Ouyang[1,2]✉, Huiming Bao[1,2], Gary R. Byerly[3] & Qiuli Li[4,5]

Compositional heterogeneity exists in Earth's deep mantle, which can be caused by the subduction of oceanic slabs. How early this process started on Earth remains highly debated due to the scarcity of early Archean materials with pristine mantle compositional signatures. Here, using the oxygen isotope and elemental compositions of fresh olivine grains in the 3.27-Ga komatiites of the Weltevreden Formation in the Barberton Greenstone Belt in Southern Africa, we discovered two groups of samples with primitive olivine grains. Group I exhibits normal mantle-like $\delta^{18}O$ values and high Fo contents ($\delta^{18}O = 4.9$–$5.4‰$; Fo = 93–95); Group II is characterized by lower $\delta^{18}O$ values with slightly lower Fo contents ($\delta^{18}O = 3.6$–$4.7‰$; Fo = 91–93). These $\delta^{18}O$ values correlate with other geochemical proxies of olivine-poor iron-rich pyroxenite sources, indicating that the Weltevreden komatiites were derived from two distinct mantle sources. The existence of the low-$\delta^{18}O$ magmas can be best explained by recycling of the altered oceanic crust into deep mantle arguably by subduction, which started 3.3 billion years ago and is responsible for the deep mantle heterogeneity in early Earth.

[1] International Center for Isotope Effects Research, Nanjing University, Nanjing 210023, China. [2] Frontiers Science Center for Critical Earth Material Cycling, State Key Laboratory for Mineral Deposits Research, School of Earth Sciences and Engineering, Nanjing University, Nanjing 210023, China. [3] Department of Geology and Geophysics, Louisiana State University, Baton Rouge, LA 70803, USA. [4] State Key Laboratory of Lithospheric Evolution, Institute of Geology and Geophysics, Chinese Academy of Sciences, Beijing 100029, China. [5] Innovation Academy for Earth Science, Chinese Academy of Sciences, Beijing 100029, China. ✉email: ouyang@nju.edu.cn

The interaction between the surface and the deep interior of Earth shapes the habitability of our planet and strongly affects the physicochemical properties of the mantle. Composition variability in mantle-derived magmas is commonly ascribed to mantle heterogeneity[1,2], which occurs via two main mechanisms. One is the 'top-down' model in which crustal materials can be introduced into the mantle by either subduction[3,4] (a hallmark of plate tectonics), to a lesser degree by delamination processes[5]. Thereinto, plate tectonics is well accepted as the paradigm for modern Earth's evolution that distinguishes Earth from other planets in the solar system and forms the most efficient mechanism to achieve mass circulation and energy exchange between Earth's crustal and mantle reservoirs. The timing of the onset of plate tectonics is intensely debated, varying from the Hadean to the late Neoproterozoic[6–8]. As an alternative, the 'bottom-up' model suggests that these heterogeneities may be inherited from the primordial mantle, which suffered early magmatic differentiation events, including magma ocean partial melting and crystallization[9], metal-silicate re-equilibration[10], or inefficient mixing[11]. These long-term isolated deep-seated reservoirs have not been homogenized through mantle convection and have persisted until today[12]. In addition, meteorite impacting as an exogenetic process is also a potential model[13].

Oxygen isotopes (expressed as $\delta^{18}O = \{(^{18}O/^{16}O)_{sample}/(^{18}O/^{16}O)_{VSMOW} - 1\}$, which are fractionated significantly only during fluid-rock interactions at shallow depths, offer a clue to the source of magma[14]. The oxygen isotope composition of the upper mantle, revealed by fresh mantle-derived rocks (mid-ocean ridge basalts (MORB), ocean island basalts (OIB), and mantle xenoliths), shows narrow variations over Earth's history, defining an average $\delta^{18}O$ value of 5.5 ± 0.5‰[15,16]. On the other hand, Mg-rich komatiites occurred almost exclusively in the Archean and are regarded as products of a high degree of partial melting of deep-seated mantle plumes, which are generally considered to originate in the lower mantle, even at the core-mantle boundary[17]. They are unique archives of the compositional and thermal state of the early deep mantle and can help constrain the nature of mantle heterogeneity, which may not be recorded in modern lavas due to the unidirectional evolution of the Earth. The oxygen isotope compositions of komatiites are poorly constrained due to their restricted preservation and susceptibility to alteration. A previous study reported low $\delta^{18}O$ values of olivine separates in ~3.3 Ga komatiites from the Barberton Greenstone Belt (BGB) by CO_2 laser fluorination, which has been interpreted as the result of magma ocean crystallization during the Hadean[18]. However, geochemical data of the old rocks from other cratons provide no compelling evidence for such an isotopically depleted or enriched mantle source before ~3.5 Ga (based on their Hf-Nd isotope records[19,20]). Likewise, the existence of recycled crustal material in the source or contamination of crustal material upon ascent can give rise to deviation from the normal $\delta^{18}O$ values of mantle-derived rocks[21]. Therefore, constraining the origin of komatiites with anomalous $\delta^{18}O$ values reveals the link between the potential deep mantle heterogeneity and geodynamic processes. In addition, the trace element chemistry of olivine can track source compositions and magma evolution[3,22,23]. Hence, the oxygen isotopic compositions of unaltered olivine grains, integrated with the chemistry and whole-rock compositions of their host rocks may help to distinguish the variable processes mentioned above.

The 3.27 Ga Weltevreden Formation in the BGB, which is part of the Kaapvaal Craton in Southern Africa, possesses some of the least altered komatiites. They belong to Al-enriched type komatiites (Al/Ti ≈ 30), which feature light rare earth element (LREE) depletion and heavy rare earth elements (HREE) enrichment[9,24]. Here, we select 11 hand samples from 6 different lava flows from the Pioneer Igneous Complex and Saw Mill areas, all of which are massive peridotitic komatiites. We obtained olivine grains from these komatiites and measured $\delta^{18}O$ using secondary ion mass spectrometry (SIMS) and laser fluorination (LF), major and minor elements using electron-probe microanalysis (EPMA), minor and trace elements using laser ablation inductively coupled plasma mass spectrometry (LA-ICP-MS), and whole-rock major-trace element (see Supplementary Methods). A detailed geological background, sample description (Supplementary Fig. 1), and location (Supplementary Data 1) can be found in Supplementary Note 1.

Results

Olivine chemistry. Most fresh olivine grains are ranging from 0.3 to 1.0 mm in size. Back-scattered electron (BSE) images show that the relict olivine cores are commonly well-preserved and no obvious core-rim zoning has been recognized (Fig. 1). We performed 383 in situ oxygen-isotope measurements of olivine by SIMS on 290 olivine grains extracted from the 11 samples. The $\delta^{18}O$ values fall in two clusters (Fig. 2). One cluster consists of 208 grains from 6 samples and displays the canonical mantle range for olivine[16] (5.18 ± 0.28‰, 2 SD) ranging from 4.68 ± 0.34‰ to 5.72 ± 0.35‰ (2δ) with an average value of 5.08 ± 0.17‰ (1 SD, $n = 208$). The other cluster consists of 175 grains from 5 samples and shows $\delta^{18}O$ values ranging from 3.56 ± 0.17‰ to 4.94 ± 0.30‰ (2δ) with an average value of 4.35 ± 0.30‰ (1 SD, $n = 175$). Likewise, olivine macrocrysts can be subdivided into two groups based on their minor-trace element contents (Supplementary Note 2; Supplementary Figs. 2 and 3). The normal-$\delta^{18}O$ olivine group is characterized by extremely high Fo contents ranging from 92.5 to 95.0; the low-$\delta^{18}O$ olivine shows slightly lower Fo contents with 90.7–92.5. There is little overlap in $\delta^{18}O$-Fo compositions between the two groups (Fig. 3). Overall, the compositional range of the low-$\delta^{18}O$ olivine cluster shows fewer scatter than those of the normal-$\delta^{18}O$ olivine cluster. Olivine grains from each sample show relatively homogenous $\delta^{18}O$-element compositions (Figs. 3 and 4). The complete oxygen isotope-element data sets of olivine and the corresponding reference materials are presented in Supplementary Data 2–6.

Discussion

The Weltevreden komatiites have experienced serpentinization and low-grade metamorphism, which could have altered the original oxygen isotope-element composition. However, no internal zoning or systematic difference in oxygen isotope-element compositions between the core-rim domains of olivine grains was observed. BSE images assisted all in situ analysis (SIMS/EPMA/LA-ICP-MS) to avoid fractures, melt inclusion, or alteration domains. The $\delta^{18}O$ values of olivine are independent of core-rim location, grain size, and degree of external alteration (as described in Supplementary Note 3). Therefore, olivine grains should have retained their original oxygen isotope compositions.

The two olivine clusters show distinct oxygen isotope-element compositions, which may indicate their different source compositions. We propose that the low-$\delta^{18}O$ olivine group crystallized from magmas with the contribution of low-$\delta^{18}O$, subducted, altered oceanic crust. Other processes, including partial melting, crustal contamination, mantle metasomatism, and melt-mineral fractionation, can also result in lowering the olivine $\delta^{18}O$ value. As we argued below, these other processes cannot explain the origin of the BGB low-$\delta^{18}O$ olivine group.

The magnitude of oxygen isotope fractionation during partial melting and melt-mineral fractionation is relatively small in peridotitic systems[25]. Strong correlations for both whole-rock

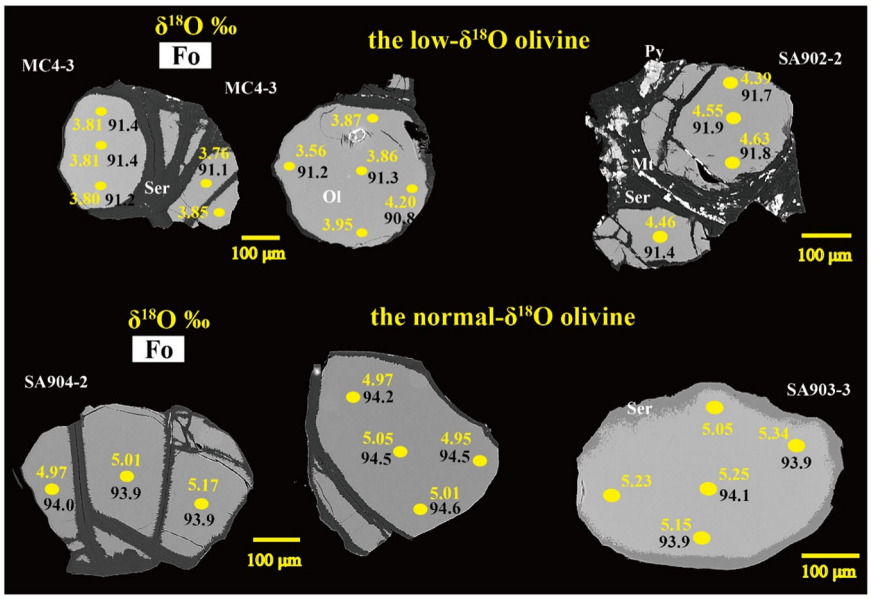

Fig. 1 Back-scattered electron (BSE) imaging of representative olivine grains in Weltevreden komatiites. Though affected by serpentinization, the unaltered core is preserved. The upper row is low $\delta^{18}O$ olivine grains; the lower row is normal $\delta^{18}O$ olivine grains. The yellow spots represent the analysis domain for $\delta^{18}O$ by SIMS and Fo by EPMA. The yellow number is the $\delta^{18}O$ value of olivine; the black number is the Fo content. Each grain shows uniform $\delta^{18}O$-Fo compositions without core-rim zoning. Ol, olivine; Ser, serpentine; Py, pyroxene; Mt, magnetite.

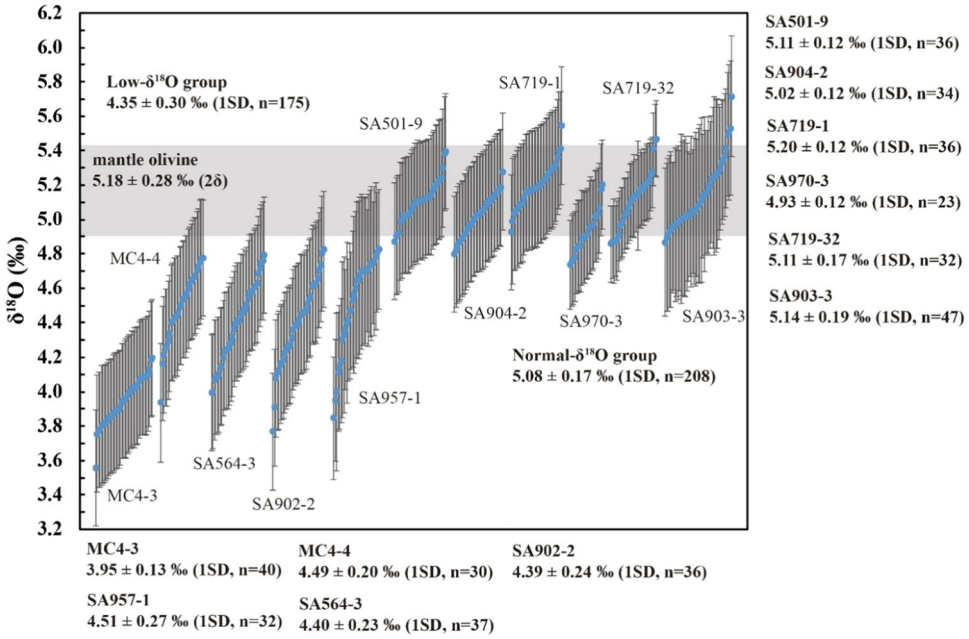

Fig. 2 A compilation of the oxygen isotope composition of all olivines analyzed by SIMS in this study. Gary band represents the mantle olivine value (5.18 ± 0.28‰, 2 SD; SD means standard deviation). Error bars indicate the 2δ of each analysis. $2\delta = SQRT((2SE)^2 + (2\,SD)^2)$, where SE is the analytical standard error of each analysis and SD is the standard deviation of the analyses of the San Carlos olivine reference material in each session and represents the 95% confidence level.

samples and olivines between MgO content and most elements indicate that olivine was the only major liquidus phase over the crystallization process (Supplementary Fig. 4; Supplementary Data 7), though the occurrence of an inflection point in the Fo versus Cr diagram implies the co-crystallization of minor Cr-rich chromite (Supplementary Fig. 3b), which are consistent with previous observation[9]. The Weltevreden komatiites were characterized by extremely high eruption temperatures (~1600 °C) and mantle potential temperatures (~1800 °C)[26,27], the oxygen-isotope fractionation between olivine and ultramafic melt at 1600 °C is assumed to be <−0.3‰, removing olivine will thus lead to an increase in $\delta^{18}O$ and a decrease in the $Mg^{\#}$ of the melt, inconsistent with the low $\delta^{18}O$-Fo olivines. Such high-temperature, low-viscosity komatiitic lavas would lead to efficient heat transfer to the surrounding wall rocks en route to the surface and could result in contamination of crustal materials. When crustal contamination and hydrothermal alteration occur, it is expected that komatiitic lavas would exhibit lower eruption temperature, elevated lithophile trace element abundances (such as Ba, Th, U, Zr, and LREE), and trends of decreasing $\delta^{18}O$ with decreasing Fo,

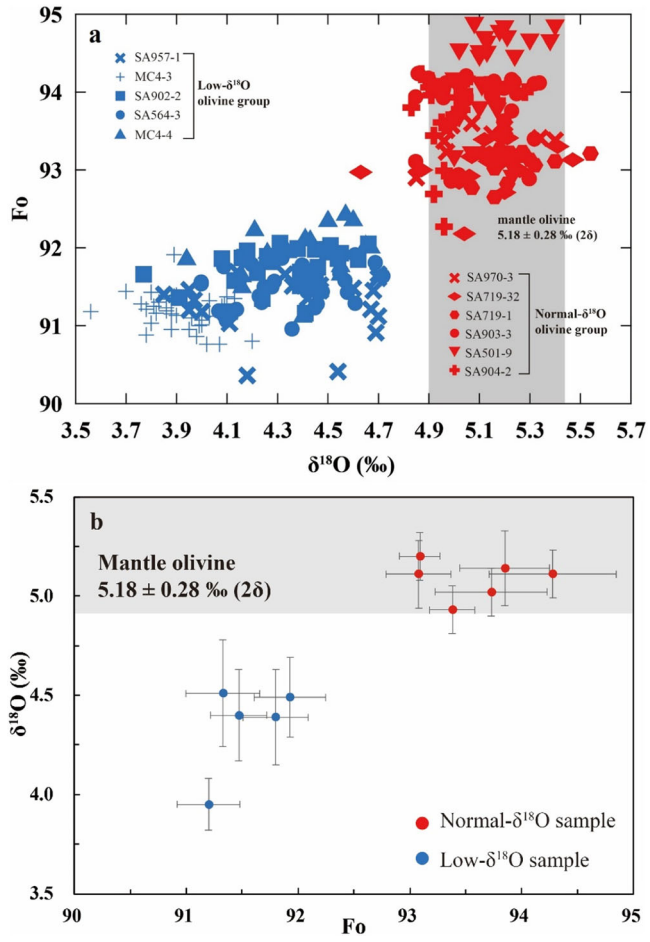

Fig. 3 Fo-$\delta^{18}O$ covariations diagrams for olivine grains. a Binary diagram of $\delta^{18}O$ value and Fo content in olivine from the Weltevreden komatiites. Blue symbols represent low $\delta^{18}O$ olivines from five samples; red symbols represent normal $\delta^{18}O$ olivine from the other six samples. **b** Average $\delta^{18}O$ values versus average Fo values in olivine from each sample. "Error bars" represent one standard deviation (1 SD) of $\delta^{18}O$ and Fo content of olivines in each sample, respectively. There is no overlap of $\delta^{18}O$-Fo systematics between the two groups.

MgO, and Zr/Nb, along with an increasing in $(La/Yb)_N$, Sm/Yb, Ba/La, and Ba/Li[28–30]. However, the observed geochemical characteristics in Weltevreden komatiites contradict these expectations, with extremely low concentrations of Ba and Th, and uniform LREE depletion (Supplementary Fig. 5), indicating no disturbance of incompatible elements. Additionally, the $\delta^{18}O$ values do not show a correlation with these crustal contamination parameters (Supplementary Fig. 6). These distinctive geochemical characteristics of olivines and host whole rocks effectively rule out crustal contamination as the cause of the low-$\delta^{18}O$ values in parental Weltevreden komatiite melts. Assimilation of low-$\delta^{18}O$ sub-continental lithospheric mantle (SCLM) materials is a possible mechanism. In such cases, olivine $\delta^{18}O$ values commonly show a strong correlation with other geochemical parameters, such as enriched in Na, Ti, Ca, Mn, and Zn, lower Fo and Ni contents, with the occurrence of olivine rims and low-Fo cores[31]. The Weltevreden olivine grains show no compositional zonation, and their restricted $\delta^{18}O$-element systematics in each olivine grain and sample with high Fo contents (>91) is inconsistent with assimilation of SCLM materials as a mechanism for the low-$\delta^{18}O$ olivine. Moreover, the distribution and volume of low-$\delta^{18}O$ SCLM material are less than those of high-$\delta^{18}O$ material[32]. It seems implausible that the proto-melt selectively interacted with low-$\delta^{18}O$ domains but not any high-$\delta^{18}O$ domains. Another possibility is the assimilation of low-$\delta^{18}O$ outer core material[33]. If so, we would expect lower Mn/Fe ratios due to the high Fe content of the core, which is not observed in the low-$\delta^{18}O$ olivines (Supplementary Fig. 7) and is inconsistent with the high Fo content of olivines.

Byerly et al.[18] proposed that the low-$\delta^{18}O$ mantle source represents an isolated deep-seated mantle domain, which underwent fractional crystallization of magma ocean minerals during the Hadean based on their Hf-Nd-Os isotope systematics[9,34]. However, geochemical features suggest that the mantle source of Weltevreden komatiites does not retain this deep crystallization event because of the lack of obvious Zr anomalies, high Hf/Sm ratios, and an unresolved ^{142}Nd anomaly in these lavas, which are inconsistent with the crystallization trends[35]. Moreover, in any fractional crystallization scheme, the assemblages will be dominated by a mixture of bridgmanite and Ca-perovskite[34,35]. There is negligible oxygen isotope fractionation among Mg_2SiO_4 polymorphs[36] (forsterite-wadsleyite-ringwoodite-bridgmanite). In addition, perovskite shows lower $\delta^{18}O$ values than olivine when equilibrated at high temperatures[37]. Therefore, precipitation of these minerals will lead to an increase in $\delta^{18}O$ values in the residual melt, ruling out this mechanism as the cause of the low-$\delta^{18}O$ olivine. A detailed assessment of our results and those of Byerly et al.[18] (Supplementary Data 8) can be found in Supplementary Note 4.

The occurrence of olivine with mantle-like $\delta^{18}O$ value in komatiites suggests oxygen isotope composition of the 3.3 Ga deep mantle domain is similar with that of the modern upper mantle. It is conceivable that they are inherited from magma oceans following the Moon-forming giant impact at 4.44 Ga, which homogenized the oxygen isotope compositions of proto-Earth and Theia[38]. The 3.55–3.30 Ga komatiites in the BGB and East Pilbara in Australia[39] and the 3.45 Ga Longwan ultramafic-mafic suite in China[40] may imply that large-scale deep mantle convection has been operating since the Paleoarchean, in favor of the homogenization of the oxygen isotope composition on the whole mantle-scale.

Deep recycling of the high-temperature hydrothermally altered oceanic crust (AOC) may provide substantial ^{18}O-depleted domains in the deep mantle. The mantle eclogite (is generally deemed as the metamorphic subducted slab's counterpart) and the AOC (as low as −2‰)[41] displays a similar variation range of $\delta^{18}O$ value (2–12‰)[42], suggesting no obvious oxygen isotope fractionation of the AOC during subduction. Both models and geological records of marine iron oxides suggest that Archean seawater had lower $\delta^{18}O$ than modern seawater[43,44]. It is reasonable to assume the $\delta^{18}O$ value of 0–2‰ for the Archean high-T AOC crust, and the ambient mantle is 5.5‰, a contribution of just 20–10% recycled material is required to form the mantle domain with low-$\delta^{18}O$ values (3.6–4.4‰) observed in our samples. This estimate is consistent with the amounts of pyroxenite-rich lithologies-derived components in sources of komatiites based on olivine-compatible element systematics[3]. On the other hand, olivine minor element systematics has been proposed as a proxy for source lithology identification, which is applied widely to the geochemical enrichment of OIBs[3,45]. The rationale behind this approach is the distinction of the modal mineralogy in both the mantle source and the residue, which plays critical roles in determining the bulk partition coefficients for elements and further the compositions of olivine. Generally, the two groups of olivine in our study display different evolutionary trends in diagrams of Fo versus some elemental concentrations and element ratios (Supplementary Fig. 7). The low-$\delta^{18}O$ olivines show higher X_{px} (weight fraction of pyroxenite-derived melt, related to

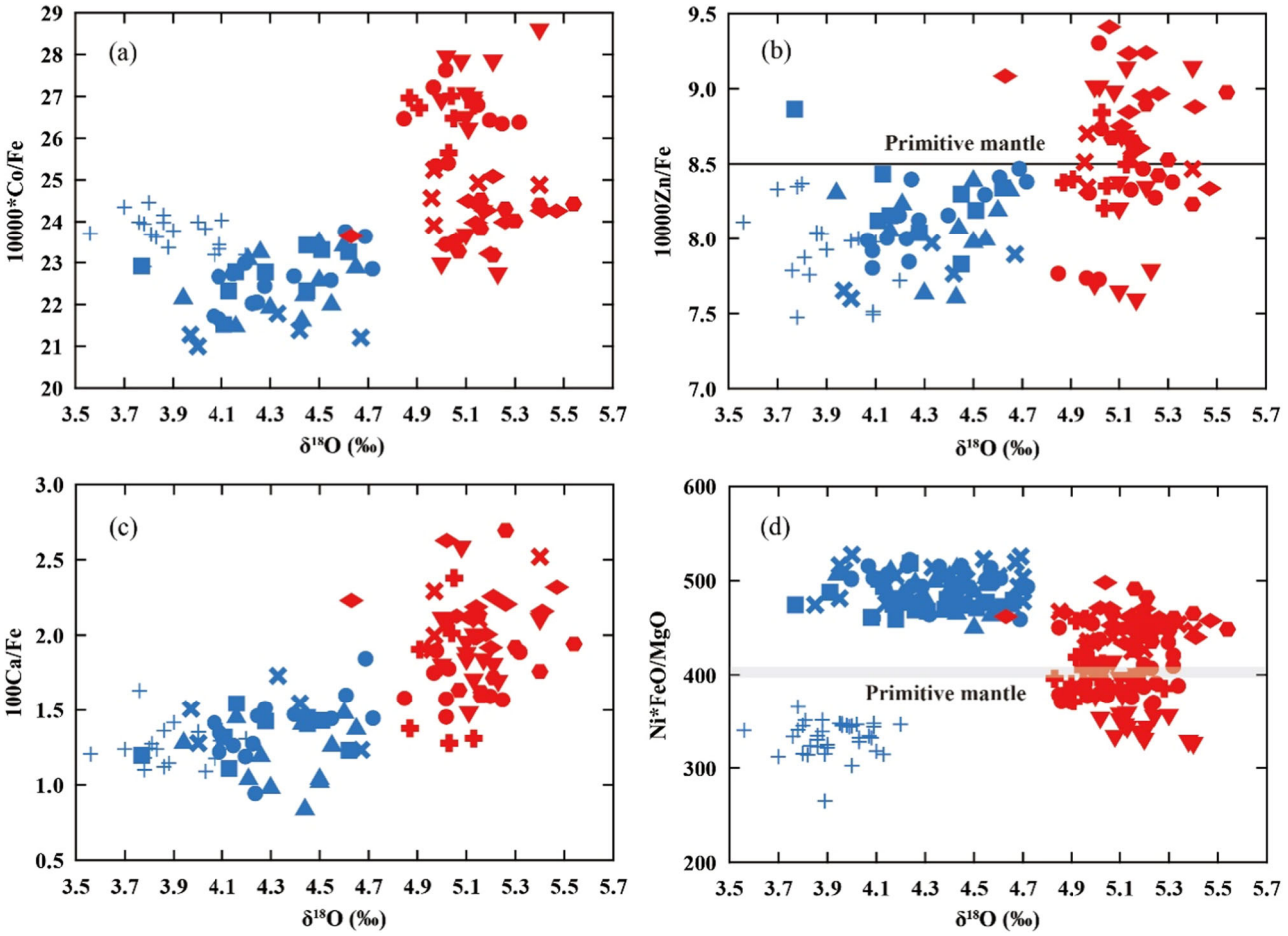

Fig. 4 $\delta^{18}O$ versus some pyroxenite-contribution proxies for olivine grains. Covariation diagrams of $\delta^{18}O$ versus **a** 10,000Co/Fe; **b** 10,000Zn/Fe; **c** 100Ca/Fe and **d** Ni*FeO/MgO for olivine in the examined Weltevreden komatiites. The compositional range of low-$\delta^{18}O$ olivine shows less scatter than normal-$\delta^{18}O$ olivine. The two groups of olivine display different trends. Overall, $\delta^{18}O$ is positively correlated with Co/Fe and Zn/Fe ratios in the low-$\delta^{18}O$ olivine. The black line in (**b**) and the gray band in (**d**) represent the 10,000Zn/Fe and Ni*FeO/MgO values of the primitive mantle, respectively.

Ni*FeO/MgO and Mn/Fe values of olivine[46]; Supplementary Fig. 8), lower 100Ca/Fe, and Co/Fe than the normal-$\delta^{18}O$ olivine (Fig. 4), consistent with the contributions of partial melts from olivine-poor mantle lithologies such as pyroxenite, garnet pyroxenite, or eclogite[3,23]. However, not all pyroxene-rich lithologies-derived proxies show differences between the two groups or correlations with $\delta^{18}O$ values; for instance, all olivine grains have similar Mn/Fe and Mn/Zn ratios. These inconsistencies indicate either decoupling or invalidation of these proxies in komatiitic systems under higher P-T conditions. Both experiments and thermodynamic models suggest that partial melts of pyroxene-rich lithologies are not very different from those of peridotite at similar melting conditions, which will hardly be detectable in the major-element patterns[47,48]. The low-$\delta^{18}O$ group samples show lower SiO_2 contents and higher FeO contents than those in the normal-$\delta^{18}O$ group samples, which is a reliable marker for the presence of pyroxene-rich lithologies in the source[48]. In addition, the buffering through garnet or clinopyroxene in pyroxenite falls off rapidly when they are exhausted in restites at high melt fractions[49,50]. The vestiges of pyroxene-rich lithologies may be diluted or even erased under these extreme scenarios, leading to an overwhelming control of compatible element contents in olivine by olivine-bearing lithologies[51].

Regardless of these complexities, oxygen isotope and elemental systematics indicate that these two groups of olivine must sample distinct mantle reservoirs, which cannot be explained by partial melting of a single mantle source, magmatic differentiation, or crustal contamination en route to the surface. The low-$\delta^{18}O$ komatiites need a modally enriched peridotite source that is depleted in ^{18}O.

Mantle enrichment by recycled crustal materials with anomalous oxygen-isotope compositions could be achieved by subduction or delamination. Delamination of dense residues after massive tonalite-trondhjemite-granodiorite (TTG) formation in the Archean would facilitate the re-fertilization of the upper mantle with a crust-like compositional signature[4]. There is no compelling evidence that these residues have $\delta^{18}O$ values lower than the normal mantle because most TTG display mantle-like $\delta^{18}O$ values[14]. In addition, this process operates in the lithospheric mantle and has no expected impact on the composition of the lower mantle where komatiite originates[5]. Therefore, the low-$\delta^{18}O$ olivines from nearly half of the BGB komatiite samples we analyzed likely reflect a deep mantle heterogeneity in early Earth.

Blobs of the subducted oceanic crust may be entrained randomly in an upwelling mantle plume, which may interact with the ambient peridotite in various ways at such high P-T conditions, and contribute to metasomatized peridotite, respective melts from the slab and peridotite, and their mixed products. The resulting metasomatic plume rises through the mantle and starts to melt when its solidus temperature is reached. Then, the melt can segregate and escape from the source once the neutral density limit is reached during adiabatic decompression, and further

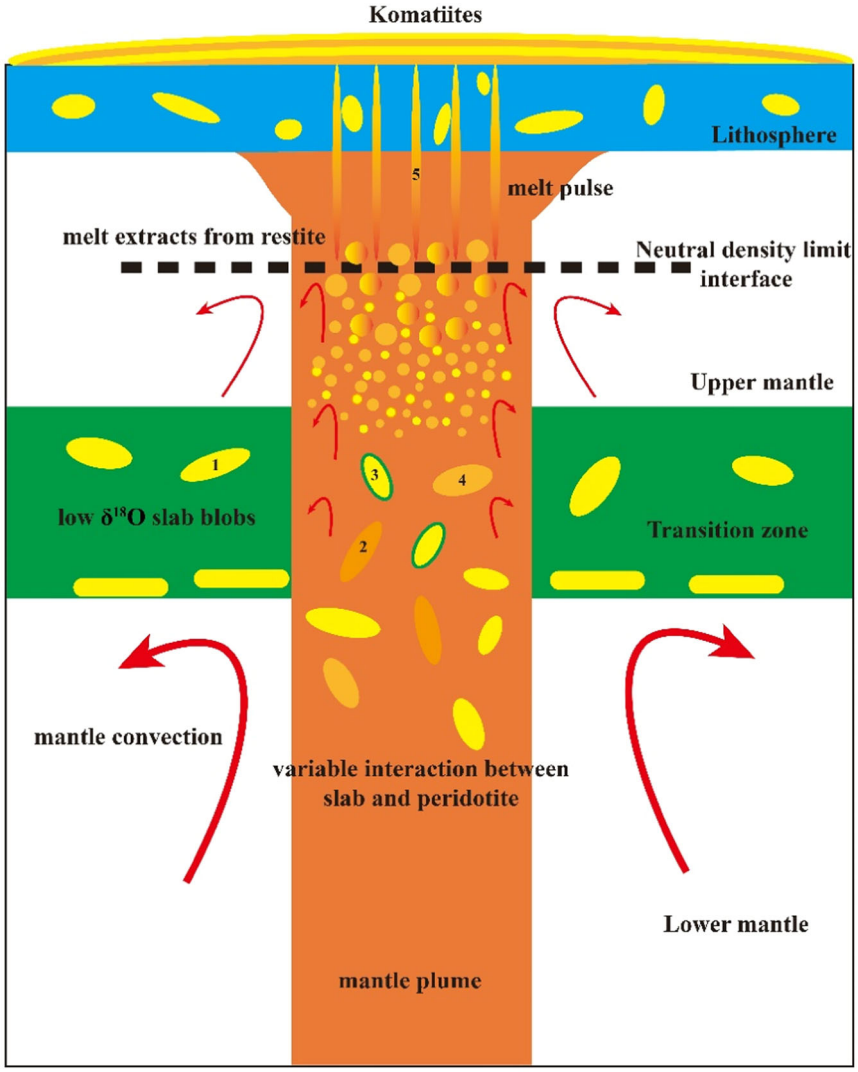

Fig. 5 Schematic illustration showing the genesis of oxygen isotope variations in the two groups of olivine in Weltevreden komatiites. Blobs of subducted oceanic crust (1, yellow) were entrained randomly in an upwelling mantle plume (orange). They can interact with the ambient peridotite in various ways in such high P-T conditions, through metasomatic peridotite (2), melts from the slab (1) and peridotite (2), and their mixing and melt-rock interaction (3, yellow core with green rim). The dotted plume traverses the mantle and starts to melt when its solidus is reached. Then, the melt (5) can segregate and escape from the source once the neutral density limit is reached during adiabatic decompression and further ascends to the surface rapidly without reaction with SCLM peridotite and crustal materials (inspired and modified after Fig. 5 in ref. [27]).

ascends to the surface rapidly without reaction with SCLM peridotite and crustal materials (Fig. 5). This model can explain the co-occurrence of low-$\delta^{18}O$ and normal-$\delta^{18}O$ komatiites, but in the different stack of flows. These results are consistent with dehydrated oceanic crust-like hydrogen (strongly negative δD values) and lithium isotope compositions of Weltevreden komatiites obtained by melt inclusions in olivine and bulk rock-olivine, respectively, suggesting a contribution of subducting dehydrated lithosphere[27,52].

The low-$\delta^{18}O$ olivine in komatiite is indicative of melt supply from a distinct ^{18}O-depleted mantle source, imparted most likely by deeply, subducted oceanic crust. A wealth of independent geological and geochemical records reflects the transformation of mantle properties (composition, thermal state, and the style of mantle convection) during the Paleoarchean-Mesoarchean, such as the widespread appearance of eclogitic inclusions diamonds[53] and paired high T/P and intermediate T/P metamorphism around 3.0 Ga[54,55]; an abrupt increase of sediments recycling tracers (e.g., Ba/La and Ba/Nb) in both basaltic and komatiitic rocks, accompanied by the rapid drop of Mg, Ni, and Cr contents in basaltic rocks since ~3.2 Ga, corresponding to distinguishable change in mantle potential temperature[4,56]; the presence of positive $\delta^{15}N$ anomalies and mass-independent fractionated sulfur isotopes from diamonds[57,58] and the evolution of komatiite compositions[17]. Combined these lines of evidence demonstrate the onset of global-scale plate tectonics in the Paleoarchean, which recycled the crustal materials into the mantle. The low-$\delta^{18}O$ Weltevreden komatiites provide an independent line of evidence supporting interaction between surficial environments and Earth's interior that started before at least 3.3 Ga and continues until the present day.

Methods

To study the compositions of olivine grains, we used the following in situ analytical techniques: secondary ion mass spectrometry (SIMS), electron probe microanalysis (EPMA), laser ablation inductively coupled plasma mass spectrometry (LA-ICP-

MS), and laser fluorination (LF). We analyzed the whole-rock major and trace elements of komatiites by X-ray fluorescence spectrometry (XRF) and LCP-MS, respectively.

SIMS. The in situ oxygen isotope analysis of olivine was carried out using a CAMECA IMS-1280 ion microprobe at the Institute of Geology and Geophysics, Chinese Academy of Sciences (IGGCAS), Beijing, China. The targets were polished and coated with gold for analysis. Cs + ions are used as the primary beam to sputter olivine for O-isotope analysis. The primary beam size is ~10*20 μm in size and was accelerated at 10 kV with an intensity of ~2 nA. An electron gun is used to compensate charging effect in the bombarding area. The ^{16}O and ^{18}O ions are detected simultaneously by two Faraday cups, and the signals are amplified by 10E10 ohms and 10E11 ohms resistors, respectively. Each analysis took 3 min, consisting of pre-sputtering, beam centering, and signal collecting. The collecting process consists of 16 cycles, and each cycle is 4 s long, which gives an average internal precision of 0.25 (2SE). The $^{18}O/^{16}O$ ratios are normalized to the Vienna Standard Mean Ocean Water standard (VSMOW) and expressed on the $\delta^{18}O$-scale. $\delta^{18}O = ((^{18}O/^{16}O)\text{sample}/(^{18}O/^{16}O)\text{standard}) - 1$. The reference material San Carlos olivine was analyzed after every six unknown samples to monitor analytical precision and to calibrate instrumental mass fractionation. The 2 SD of $\delta^{18}O$ values for San Carlos olivine measured by SIMS was 0.17–0.32‰ in all sessions. The San Carlos olivine $\delta^{18}O$ value of 5.25‰ is recommended for correcting instrument mass fractionation. Detailed analytical procedures are described by refs. [59,60]. Previous studies have undertaken detailed work on SIMS matrix effects showing oxygen-isotope variations in olivine as a function of Fe molar fractions and demonstrated a parabolic correlation between instrumental fractionation of $^{18}O/^{16}O$ and Fo values[61]. However, in olivine with Fo contents of 100–75, instrumental fractionation was found to be too small to be resolvable. For example, ref. [62] observed a systematic difference in instrumental mass fractionation (IMF) for San Carlos (Fo90) and CI114 (Fo74) olivine grains of 0.12‰, which corresponds to 0.0075‰ of IMF per each Fo number. The olivine grains analyzed in this study are characterized by high Fo contents with limited variations (95–91), and the potential IMF is less than 0.03‰, which is negligible and within the error of our measurements.

EPMA. Petrographic textures in the olivine grains were observed using a Zeiss Supra55 scanning electron microscope under the backscattering electron (BSE) mode at the IGGCAS. An energy-dispersive spectrometer (EDS) installed on this SEM was used to qualitatively identify mineral phases in the polished section. Olivine grains were analyzed quantitatively for major and minor elements on a JEOL 8230 microprobe installed with wavelength dispersive spectrometers at the State Key Laboratory for Mineral Deposits Research at Nanjing University, Nanjing, China. Each olivine grain was analyzed in the geometrical center at 15 kV accelerating voltage and probe current of 100 nA, with a spot size of 2 μm. The diffracting crystals used for the analyses include two TAP for Si, Mg, and Al (Kα); a LIF for Fe; a LIFH for Cr, and Ni (Kα); a PETJ for Ca (Kα); and a LIFI for Mn (Kα). Peak counting times include 20 s on the peak for Si, Mg, and Fe; 90 s for Cr, Ca, Mn, and Ni; and 60 s for Al. The background counting time is half of the peak counting time for each element. The total time of analysis for a single point is 8 min. Instrumental drift was monitored by analyzing San Carlos olivine twice every 20 analyses. Matrix correction and elemental quantification were undertaken using the phi-rho-Z matrix correction.

The high accuracy of the EPMA method for minor elements in olivine was previously confirmed by comparing the results of EPMA analyses with data from LA-ICP-MS. For each element, the measured concentration plots on the one-to-one line within the internal precision of both methods, as shown by error bars. Considering the known compositional heterogeneity of olivine phenocrysts, we conclude that both methods provide consistent results.

LA-ICP-MS. Trace-element concentrations in olivine and serpentine grains were acquired using the LA-ICPMS setup, a system consisting of ASI RESOlution S-155 193 nm ArF Excimer laser coupled to Thermo Scientific iCAP Qc quadrupole ICP-MS at Nanjing University, Nanjing, China. The ICPMS instrument was tuned using NIST610 standard glass to yield Th/U ratios of unity and low oxide production rates (ThO + /Th + typically < 0.15%). Carrier gas was He (~0.8 liter per min) with the addition of H_2 (0.014 liters per min), which was mixed with Ar (0.85 liters per min) before introduction into the spectrometer.

16 isotopes (^{25}Mg, ^{27}Al, ^{29}Si, ^{31}P, ^{43}Ca, ^{45}Sc, ^{47}Ti, ^{51}V, ^{53}Cr, ^{57}Fe, ^{55}Mn, ^{59}Co, ^{60}Ni, 65Cu, 66Zn, and 232Th) were monitored. Spot size, pulse frequency/laser repetition rate, and laser fluence were 29 μm, 5 Hz, and 3.8 J/cm^2, respectively. Each analysis was performed in time-resolved mode and included 20 s of background measurement, 50 s sample ablation, and 20 s of washout. A full analytical session typically comprised blocks of 3 standard analyses (two NIST610 standard glass, and one NIST612 standard glass) followed by 8 olivine unknown samples. NIST 610 was used as the primary trace-element calibration standard and NIST 612 was used as the secondary trace-element calibration standard. Detailed analytical procedures are described in ref. [63]. Data reduction and production of trace-element distribution line profiles were undertaken using ICPMSData version 12.0. ^{29}Si was used as an internal standard to account for variations in ablation yield. Elemental abundances were determined using the USGS glass reference material NIST 610 as a bracketing standard. The reference material BCR-2G, GSE-1G, and San Carlos olivine were analyzed as unknowns to assess the accuracy and precision of the analyses. Repeated BCR-2G and GSE-1G analyses during this study show that the accuracy for most elements and/or masses is ≤5% when compared to the recommended published values from the GeoReM Database (website: GeoRe, - Database on geochemical, environmental and biological reference materials (gwdg.de)).

Laser fluorination. Triple oxygen isotope compositions were measured at the International Center for Isotope Effects Research (ICIER) at Nanjing University. Olivine grains were selected, washed, and crushed to a fine fraction (~150 μm). Approximately 2.5–3 mg of olivine was loaded onto stainless steel holders along with the standard reference material San Carlos olivine. The O_2 extraction from rock samples followed the procedure detailed by ref. [64]. Briefly, the olivine samples are reacted with BrF5 assisted by CO_2 laser heating to generate O_2 gas. The produced O_2 is purified by three liquid nitrogen traps and subsequently collected onto a 5 Å molecular sieve. The purified O_2 is then expanded into the sample bellows of a Thermo MAT 253 Plus mass spectrometer, and measured against a reference gas in dual inlet mode. Each measurement consists of three acquisitions, and each acquisition includes 8 sample/reference cycles. The pressure of the sample and reference bellows are all adjusted to about 5 V on mass 33 at the beginning of each acquisition. The reference gas was calibrated to O_2 liberated from silicate standards KRS and SKFS using the same fluorination line, and triple oxygen isotope compositions in KRS and SKFS are calibrated to VSMOW previously[65].

Whole-rock major and trace elements. The major element compositions were measured by Axios X-ray fluorescence spectrometry (XRF-1500) associated with the Claisse M4 gas fluxer at the IGGCAS. Approximately 0.50 g of rock powder was first ignited at 1050 °C for approximately 1 h to obtain the loss on ignition (LOI). Oxide compositions of all the samples have been recalculated to 100% on an anhydrous basis. The BHVO-2 and AGV-2 standard materials are used for calibration. Uncertainties were better than 1 wt%. Trace element analysis of whole rock was conducted on Agilent 7700e ICP-MS at the State Key Laboratory of Geological Processes and Mineral Resources (GPMR), China University of Geosciences in Wuhan (CUGW), Wuhan, China. The detailed sample-digesting procedure was as follows ref. [66]: (1) Sample powder (200 mesh) was placed in an oven at 105 °C for drying of 12 h; (2) 50 mg sample powder was accurately weighed and placed in a Teflon bomb; (3) 1 ml HNO_3 and 1 ml HF were slowly added into the Teflon bomb; (4) Teflon bomb was put in a stainless steel pressure jacket and heated to 190 °C in an oven for >24 h; (5) After cooling, the Teflon bomb was opened and placed on a hotplate at 140 °C and evaporated to incipient dryness, and then 1 ml HNO_3 was added and evaporated to dryness again; (6) 1 ml of HNO_3, 1 ml of MQ water and 1 ml internal standard solution of 1 ppm In was added, and the Teflon bomb was resealed and placed in the oven at 190 °C for >12 h; (7) The final solution was transferred to a polyethylene bottle and diluted to 100 g by the addition of 2% HNO_3. The BHVO-2, AGV-2, and W-2A standard materials are used for calibration. The precision of trace-element analyses was better than ~3%.

Data availability

All data used to support the findings of this study have been deposited in the public repository figshare (https://doi.org/10.6084/m9.figshare.24845151.v1).

Received: 8 August 2023; Accepted: 21 December 2023;
Published online: 12 January 2024

References

1. Hofmann, A. W. Mantle geochemistry: the message from oceanic volcanism. *Nature* **385**, 219–229 (1997).
2. Zindler, A. & Hart, S. Chemical geodynamics. *Ann. Rev. Earth Planet. Sci.* **14**, 493–571 (1986).
3. Sobolev, A. V. et al. The amount of recycled crust in sources of mantle-derived melts. *Science* **316**, 412–417 (2007).
4. Gamal El Dien, H., Doucet, L. S., Murphy, J. B. & Li, Z. X. Geochemical evidence for a widespread mantle re-enrichment 3.2 billion years ago: implications for global-scale plate tectonics. *Sci. Rep.* **10**, 9461 (2020).
5. Bédard, J. H. Stagnant lids and mantle overturns: implications for Archaean tectonics, magma genesis, crustal growth, mantle evolution, and the start of plate tectonics. *Geosci. Front.* **9**, 19–49 (2018).
6. Brown, M., Johnson, T. & Gardiner, N. J. Plate tectonics and the Archean Earth. *Annu. Rev. Earth Pl Sc.* **48**, 291–320 (2020).
7. Cawood, P. A. et al. Geological archive of the onset of plate tectonics. *Philos. Trans. A Math. Phys. Eng. Sci.* **376**, 20170405 (2018).
8. Stern, R. J. The evolution of plate tectonics. *Philos. Trans. A Math. Phys. Eng. Sci.* **376**, 20170406 (2018).
9. Puchtel, I. S. et al. Insights into early Earth from Barberton komatiites: evidence from lithophile isotope and trace element systematics. *Geochim. Cosmochim. Acta* **108**, 63–90 (2013).
10. Rubie, D. C. et al. Highly siderophile elements were stripped from Earth's mantle by iron sulfide segregation. *Science* **353**, 1141–1144 (2016).
11. Maier, W. D. et al. Progressive mixing of meteoritic veneer into the early Earth's deep mantle. *Nature* **460**, 620–623 (2009).
12. Mukhopadhyay, S. & Parai, R. Noble gases: a record of Earth's evolution and mantle. *Dynamics* **47**, 389–419 (2019).
13. Johnson, T. E. et al. Giant impacts and the origin and evolution of continents. *Nature* **608**, 330–335 (2022).
14. Valley, J. W. et al. 4.4 billion years of crustal maturation: oxygen isotope ratios of magmatic zircon. *Contrib. Mineral. and Petrol.* **150**, 561–580 (2005).
15. Eiler, J. M. Oxygen isotope variations of basaltic lavas and upper mantle rocks. *Rev. Mineral. Geochem.* **43**, 319–364 (2001).
16. Mattey, D., Lowry, D. & Macpherson, C. Oxygen isotope composition of mantle peridotite. *Earth Planet. Sci. Lett.* **128**, 231–241 (1994).
17. Arndt, N. in *Komatiite* (eds Lesher, C. M., Arndt, N. & Barnes, S. J.) 233–234 (Cambridge University Press, 2008).
18. Byerly, B. L., Kareem, K., Bao, H. & Byerly, G. R. Early Earth mantle heterogeneity revealed by light oxygen isotopes of Archaean komatiites. *Nat. Geosci.* **10**, 871–875 (2017).
19. Murphy, D. et al. Combined Sm-Nd, Lu-Hf, and 142Nd study of Paleoarchean basalts from the East Pilbara Terrane, Western Australia. *Chem. Geol.* **578**, 120301 (2021).
20. Salerno, R., Vervoort, J., Fisher, C., Kemp, A. & Roberts, N. The coupled Hf-Nd isotope record of the early Earth in the Pilbara Craton. *Earth Planet. Sci. Lett.* **572**, 117139 (2021).
21. Taylor, H. P. The effects of assimilation of country rocks by magmas on 18O/16O and 87Sr/86Sr systematics in igneous rocks. *Earth Planet. Sci. Lett.* **47**, 243–254 (1980).
22. Foley, S. F., Prelevic, D., Rehfeldt, T. & Jacob, D. E. Minor and trace elements in olivines as probes into early igneous and mantle melting processes. *Earth Planet. Sci. Lett.* **363**, 181–191 (2013).
23. Le Roux, V., Dasgupta, R. & Lee, C. T. A. Mineralogical heterogeneities in the Earth's mantle: constraints from Mn, Co, Ni and Zn partitioning during partial melting. *Earth Planet. Sci. Lett.* **307**, 395–408 (2011).
24. Thompson Stiegler, M., Cooper, M., Byerly, G. R. & Lowe, D. R. Geochemistry and petrology of komatiites of the Pioneer Ultramafic Complex of the 3.3Ga Weltevreden Formation, Barberton greenstone belt, South Africa. *Precambrian Res.* **212–213**, 1–12 (2012).
25. Bindeman, I. N., Ionov, D. A., Tollan, P. M. E. & Golovin, A. V. Oxygen isotope (δ18O, Δ′17O) insights into continental mantle evolution since the Archean. *Nat. Commun.* **13**, 3779 (2022).
26. Connolly, B. D. et al. Highly siderophile element systematics of the 3.3Ga Weltevreden komatiites, South Africa: Implications for early Earth history. *Earth Planet. Sci. Lett.* **311**, 253–263 (2011).
27. Sobolev, A. V. et al. Deep hydrous mantle reservoir provides evidence for crustal recycling before 3.3 billion years ago. *Nature* **571**, 555–559 (2019).
28. Day, J. M. D. Evidence against an ancient non-chondritic mantle source for North Atlantic Igneous Province lavas. *Chem. Geol.* **440**, 91–100 (2016).
29. Genske, F. S. et al. Oxygen isotopes in the Azores islands: crustal assimilation recorded in olivine. *Geology* **41**, 491–494 (2013).
30. Giuliani, A. Insights into kimberlite petrogenesis and mantle metasomatism from a review of the compositional zoning of olivine in kimberlites worldwide. *Lithos* **312–313**, 322–342 (2018).
31. Xu, J.-Y. et al. Light oxygen isotopes in mantle-derived magmas reflect assimilation of sub-continental lithospheric mantle material. *Nat. Commun.* **12**, 6295 (2021).
32. Fitzpayne, A. et al. Evidence for subduction-related signatures in the southern African lithosphere from the N-O isotopic composition of metasomatic mantle minerals. *Geochim. Cosmochim. Acta* **266**, 237–257 (2019).
33. Macpherson, C. G., Hilton, D. R., Mattey, D. P. & Sinton, J. M. Evidence for an 18O-depleted mantle plume from contrasting 18O/16O ratios of back-arc lavas from the Manus Basin and Mariana Trough. *Earth Planet. Sci. Lett.* **176**, 171–183 (2000).
34. Puchtel, I. S., Walker, R. J., Touboul, M., Nisbet, E. G. & Byerly, G. R. Insights into early Earth from the Pt–Re–Os isotope and highly siderophile element abundance systematics of Barberton komatiites. *Geochim. Cosmochim. Acta* **125**, 394–413 (2014).
35. Boyet, M., Garçon, M., Arndt, N., Carlson, R. W. & Konc, Z. Residual liquid from deep magma ocean crystallization in the source of komatiites from the ICDP drill core in the Barberton Greenstone Belt. *Geochim. Cosmochim. Acta* **304**, 141–159 (2021).
36. Wu, Z., Huang, F. & Huang, S. Isotope fractionation induced by phase transformation: first-principles investigation for Mg2SiO4. *Earth Planet. Sci. Lett.* **409**, 339–347 (2015).
37. Zheng, Y.-F. Prediction of high-temperature oxygen isotope fractionation factors between mantle minerals. *Phys. Chem. Miner.* **24**, 356–364 (1997).
38. Young, E. D. et al. Oxygen isotopic evidence for vigorous mixing during the Moon-forming giant impact. *Science* **351**, 493–496 (2016).
39. Sossi, P. A. et al. Petrogenesis and geochemistry of Archean komatiites. *J. Petrol.* **57**, 147–184 (2016).
40. Wang, C. et al. Palaeoarchaean deep mantle heterogeneity recorded by enriched plume remnants. *Nat. Geosci.* **12**, 672–678 (2019).
41. Gao, Y. et al. Downhole variation of lithium and oxygen isotopic compositions of oceanic crust at East Pacific Rise, ODP Site 1256. *Geochem. Geophys. Geosyst.* **13**, https://doi.org/10.1029/2012GC004207 (2012).

42. Korolev, N. M., Melnik, A. E., Li, X.-H. & Skublov, S. G. The oxygen isotope composition of mantle eclogites as a proxy of their origin and evolution: a review. *Earth Sci. Rev.* **185**, 288–300 (2018).
43. Galili, N. et al. The geologic history of seawater oxygen isotopes from marine iron oxides. *Science* **365**, 469–473 (2019).
44. Guo, M., Wostbrock, J. A. G., Planavsky, N. J. & Korenaga, J. Reconstructing seawater δ18O and Δ′17O values with solid Earth system evolution. *Earth Planet. Sci. Lett.* **592**, https://doi.org/10.1016/j.epsl.2022.117637 (2022).
45. Herzberg, C. Identification of source lithology in the Hawaiian and Canary Islands: implications for origins. *J. Petrol.* **52**, 113–146 (2011).
46. Gurenko, A. A., Sobolev, A. V., Hoernle, K. A., Hauff, F. & Schmincke, H.-U. Enriched, HIMU-type peridotite and depleted recycled pyroxenite in the Canary plume: a mixed-up mantle. *Earth Planet. Sci. Lett.* **277**, 514–524 (2009).
47. Lambart, S., Baker, M. B. & Stolper, E. M. The role of pyroxenite in basalt genesis: Melt-PX, a melting parameterization for mantle pyroxenites between 0.9 and 5 GPa. *J. Geophys. Res. Solid Earth* **121**, 5708–5735 (2016).
48. Lambart, S., Laporte, D. & Schiano, P. Markers of the pyroxenite contribution in the major-element compositions of oceanic basalts: review of the experimental constraints. *Lithos* **160-161**, 14–36 (2013).
49. Davis, F. A., Humayun, M., Hirschmann, M. M. & Cooper, R. S. Experimentally determined mineral/melt partitioning of first-row transition elements (FRTE) during partial melting of peridotite at 3GPa. *Geochim. Cosmochim. Acta* **104**, 232–260 (2013).
50. Walter, M. J. Melting of garnet peridotite and the origin of komatiite and depleted lithosphere. *J. Petrol.* **39**, 29–60 (1998).
51. Neave, D. A., Shorttle, O., Oeser, M., Weyer, S. & Kobayashi, K. Mantle-derived trace element variability in olivines and their melt inclusions. *Earth Planet. Sci. Lett.* **483**, 90–104 (2018).
52. Kareem, K. *Komatiites of the Weltevreden Formation, Barberton Greenstone Belt, South Africa: Implications for the Chemistry and Temperature of the Archean Mantle*. PHD thesis, Louisiana State Univ (2005).
53. Shirey, S. B. & Richardson, S. H. Start of the Wilson cycle at 3 Ga shown by diamonds from subcontinental mantle. *Science* **333**, 434–436 (2011).
54. Brown, M. & Johnson, T. Secular change in metamorphism and the onset of global plate tectonics. *Am. Min.* **103**, 181–196 (2018).
55. Zheng, Y.-F. & Zhao, G. Two styles of plate tectonics in Earth's history. *Sci. Bull.* **65**, 329–334 (2020).
56. Gamal El Dien, H., Doucet, L. S., Li, Z.-X., Cox, G. & Mitchell, R. Global geochemical fingerprinting of plume intensity suggests coupling with the supercontinent cycle. *Nat. Commun.* **10**, 5270 (2019).
57. Smart, K. A., Tappe, S., Stern, R. A., Webb, S. J. & Ashwal, L. D. Early Archaean tectonics and mantle redox recorded in Witwatersrand diamonds. *Nat. Geosci.* **9**, 255–259 (2016).
58. Smit, K. V., Shirey, S. B., Hauri, E. H. & Stern, R. A. Sulfur isotopes in diamonds reveal differences in continent construction. *Science* **364**, 383–385 (2019).
59. Tang, G. et al. Deciphering the physical mechanism of the topography effect for oxygen isotope measurements using a Cameca IMS-1280 SIMS. *J. Anal. At. Spectrom.* **30**, 950–956 (2015).
60. Tang, G. Q. et al. High-Mg# olivine, clinopyroxene and orthopyroxene reference materials for in situ oxygen isotope determination. *Geostand. Geoanal. Res.* **43**, 585–593 (2019).
61. Isa, J. et al. Quantification of oxygen isotope SIMS matrix effects in olivine samples: correlation with sputter rate. *Chem. Geol.* **458**, 14–21 (2017).
62. Bindeman, I., Gurenko, A., Sigmarsson, O. & Chaussidon, M. Oxygen isotope heterogeneity and disequilibria of olivine crystals in large volume Holocene basalts from Iceland: Evidence for magmatic digestion and erosion of Pleistocene hyaloclastites. *Geochim. Cosmochim. Acta* **72**, 4397–4420 (2008).
63. Liu, Y. et al. In situ analysis of major and trace elements of anhydrous minerals by LA-ICP-MS without applying an internal standard. *Chem. Geol.* **257**, 34–43 (2008).
64. Bao, H. & Thiemens, M. H. Generation of O_2 from $BaSO_4$ using a CO_2—laser fluorination system for simultaneous analysis of $\delta^{18}O$ and $\delta^{17}O$. *Anal. Chem.* **72**, 4029–4032 (2000).
65. Miller, M. F. et al. Mass-independent fractionation of oxygen isotopes during thermal decomposition of divalent metal carbonates: Crystallographic influence, potential mechanism and cosmochemical significance. *Chem. Geol.* **586**, 120500 (2021).
66. Liu, Y., Zong, K., Kelemen, P. B. & Gao, S. Geochemistry and magmatic history of eclogites and ultramafic rocks from the Chinese continental scientific drill hole: subduction and ultrahigh-pressure metamorphism of lower crustal cumulates. *Chem. Geol.* **247**, 133–153 (2008).

Acknowledgements

This research was supported by grants from the National Natural Science Foundation of China (NSFC, 42102245 to D.-J.O.Y., 42225301 to Q.-L.L.). The authors acknowledge Hong-Xia Ma for preparing sample mounts, Yang He for the EPMA analyses, Huan Hu for the LA-ICP-MS analyses, and Guo-Qiang Tang, Yu Liu, Xiao-Xiao Ling, and Jiao Li for the SIMS analyses, Yong-Bo Peng for sorting and shipping these samples. No sampling permissions were required.

Author contributions

D.-J.O.Y. and H.-M.B. conceived and developed the project. D.-J.O.Y. led writing of this paper, performed analyses, and data processing. G.B. carried out field investigations and sampling. Q.-L.L. contributed data and SIMS analysis. All authors contributed to editing and discussion of the paper.

Competing interests

The authors declare no competing interests.

Additional information

Supplementary information The online version contains supplementary material available at https://doi.org/10.1038/s43247-023-01197-3.

Correspondence and requests for materials should be addressed to Dongjian Ouyang.

Peer review information *Communications Earth & Environment* thanks Hamed Gamaleldien and the other, anonymous, reviewer(s) for their contribution to the peer review of this work. Primary Handling Editors: Renbiao Tao, Joe Aslin and Aliénor Lavergne. Peer reviewer reports are available.

Reprints and permission information is available at http://www.nature.com/reprints

Publisher's note Springer Nature remains neutral with regard to jurisdictional claims in published maps and institutional affiliations.